CHAPTER 6

Microstructure, Mechanical and Wear Properties of ABO_w-Al Matrix Composites

The present chapter was undertaken to characterize the microstructural features, and the consequent mechanical properties developed in aluminium borate whisker (ABO_w) reinforced (5, 10, 15 wt.%) commercially pure aluminium composites fabricated by conventional powder metallurgy technique. The aluminium powder and the whisker are effectively blended by a semi-powder metallurgy method [111]. The blended powder mixtures were cold compacted and sintered at 600°C. The sintered composites were characterized for microstructural features by optical microscopy (OM), scanning electron microscopy (SEM), energy dispersive spectroscopy (EDS), transmission electron microscopy (TEM) and X-ray diffraction (XRD) analysis. % porosity in the composites with variation in ABO_w contents was determined. The effect of variation in wt.% ABO_w on mechanical properties viz. The composites' hardness, bending strength, and compressive strength have been evaluated. The dry sliding wear behaviour is evaluated at varying sliding distances at constant loads.

6.1.Morphology and phase identification of ABO whiskers

The average diameters of the whiskers are observed to be ranging from 0.3 to 0.8 μm (from the last chapter) in **Figure 6.1**. It was difficult to separate the whiskers from the bulk due to the moderately high bonding strength. So, the exact measurement of the accurate length was not possible. However, the approximate range of the length of whiskers is pretty high about 15 to 20 μm (from last chapter). The whisker thickness was relatively homogeneous for each material. **Figure 6.2** shows the XRD patterns of the ABO whisker calcined at 1300°C.

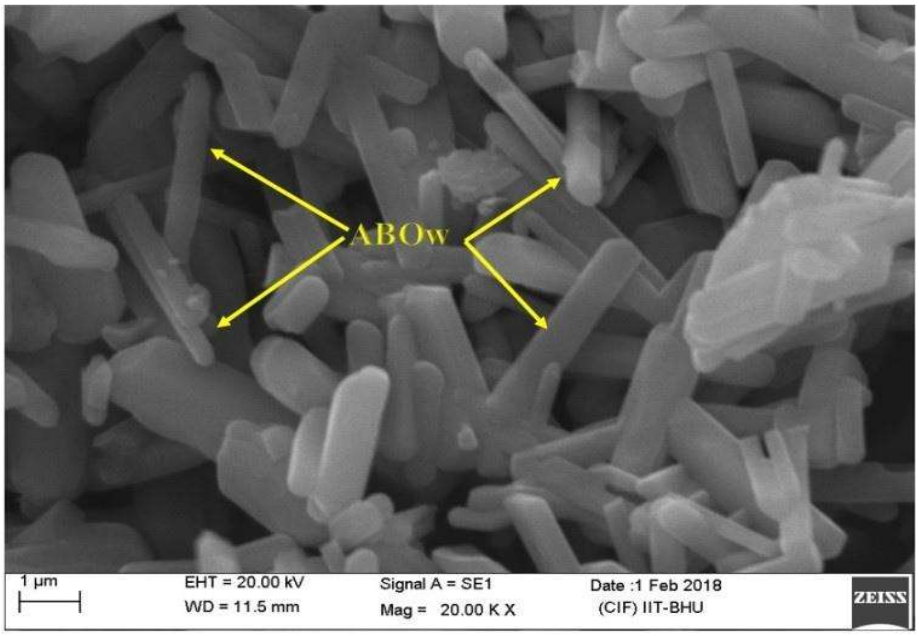

Figure 6.1: SEM image of ABO whiskers calcined at 1300°C used as reinforcement

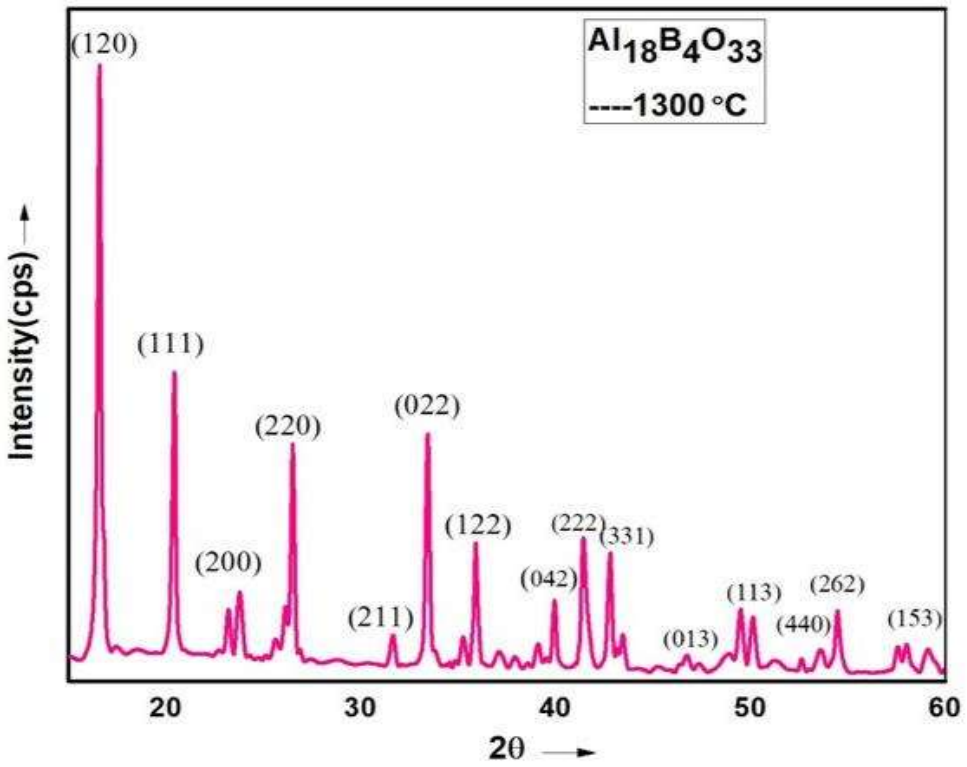

Figure.6.2: XRD pattern of ABO whisker calcined at 1300°C

The identified diffracted peaks correspond to aluminium borates ($Al_{18}B_4O_{33}$) referred from JCPDS (32-0003). The TEM bright-field images with corresponding diffraction patterns of ABO_w powder were prepared by the hydrolysis method as shown in **Figure 6.3 (a&b)**. The morphological and discontinuous structure of the micro whiskers [112] were characterized and the crystal parameters are determined as a=7.6874 Å, b=15.0127 Å, and c=5.6643Å. The parameters confirm the orthorhombic crystal structure of ABO_w reinforcements.

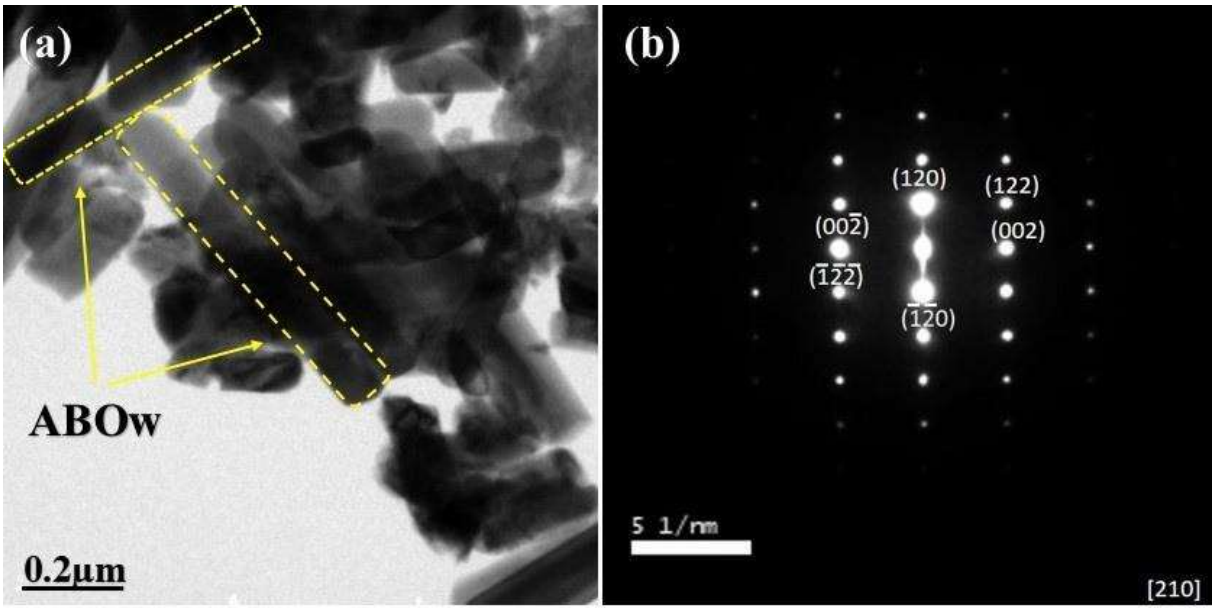

Figure 6.3: (a) TEM bright-field image and **(b)** corresponding SAED of ABO whiskers

6.2 Microstructural characterization and phase identification of composites

The scanning electron micrographs of base metal and composites are shown in **Figure 6.4**. The scanning electron micrographs show distributions of ABO whiskers throughout the volume of the composites. It is evident from the XRD patterns **Figure**

6.5 of the composites that, except aluminium and $Al_{18}B_4O_{33}$ type of aluminium borate whiskers, no other phases are present in the fabricated composites.

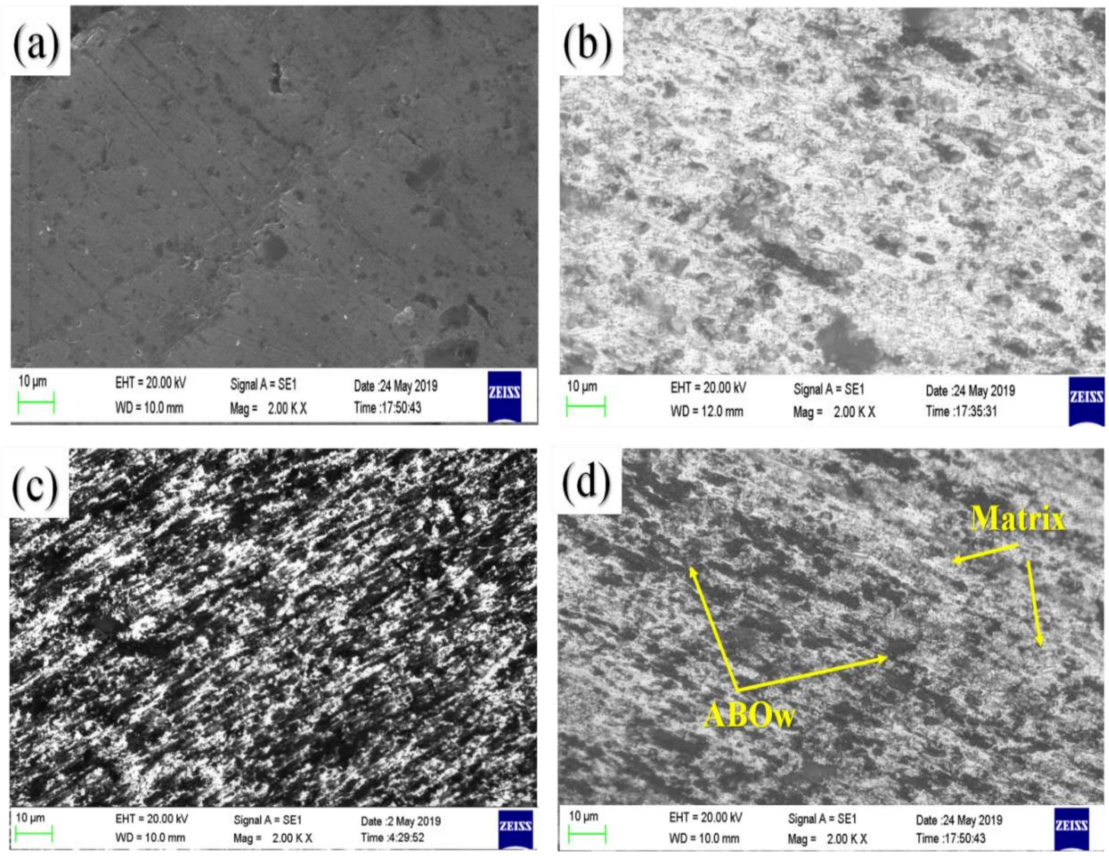

Figure 6.4: SEM micrographs of **(a)** aluminium base metal and Al-ABO_w composite with **(b)** 5 wt.% ABO whiskers; **(c)** 10 wt.% ABO_w and **(d)** 15 wt.% ABO whiskers

This confirms the absence of any whisker/matrix interface reaction during the sintering of the cold compacts. A similar observation has been reported [113]. As the volume content of ABO_w increases, the intensity of ABO_w peaks increases, whereas aluminium peaks decrease.

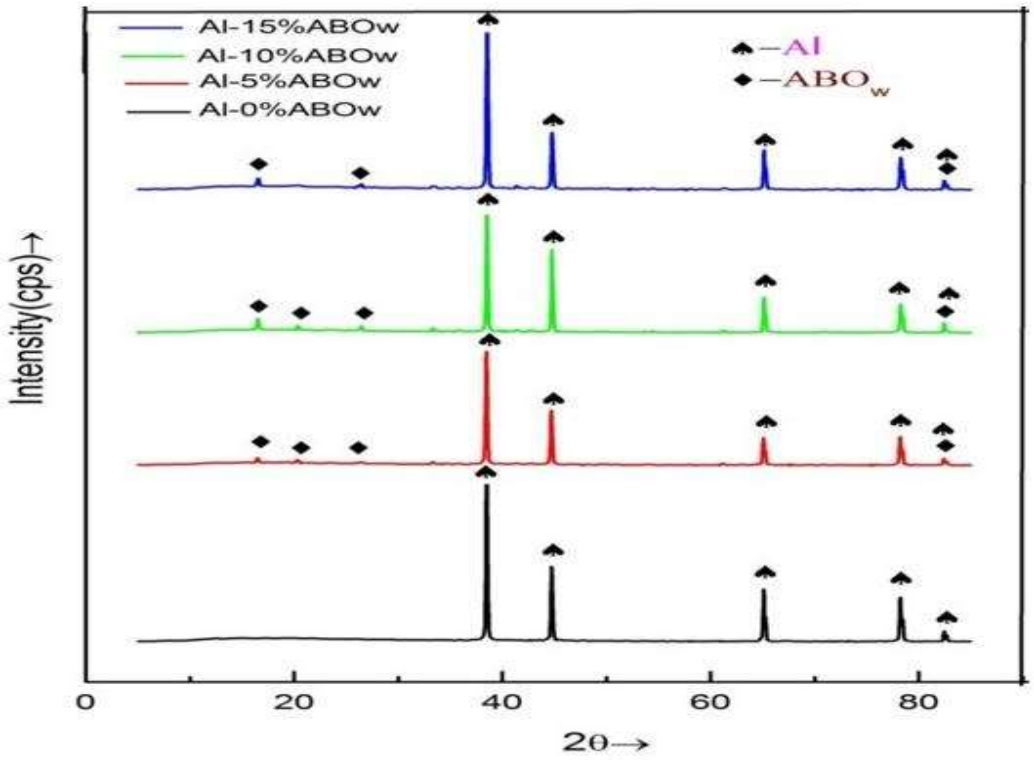

Figure 6.5: XRD patterns of sintered Al-ABO_w composites with different compositions

6.3. Measurement of density and porosity

The average porosities of the Al-ABO_w composites with varying wt. % of ABO_w are calculated from experimentally determined densities and theoretical densities, shown in **Table 6.1**. Although ABO whiskers have densities (2.94 g/cc.) [53], are slightly higher than aluminium (2.67 g/cc.), with increasing wt. % of ABO_w the composite densities are decreasing [153]. This is due to more % porosities incorporated with a higher volume of ABO_w. It is evident from the table that the average porosity increases with increasing wt. % of ABO_w.

Table 6.1: Densities and porosities of composite samples

Sample	Experiment Number	Experimental density(g/cc)	Average Theoretical density ($\rho_{th}=V_f\rho_f+V_m\rho_m$)	Average porosity (%)
Base metal Al	1	2.56	2.70	5.43
	2	2.53		
	3	2.58		
Al-5%ABOw	1	2.47	2.65	7.48
	2	2.48		
	3	2.45		
Al-10%ABOw	1	2.32	2.61	11.17
	2	2.30		
	3	2.29		
Al-15%ABOw	1	2.30	2.57	12.86
	2	2.28		
	3	2.27		

6.4. Evaluation of mechanical properties

6.4.1. Vickers hardness and bending strength

The hardness values of Al base metal and the Al-ABO_w composites are shown in **Table 6.2**. The composites' hardness was observed to increase with an increasing percentage of ABO whiskers in the composites. This may be due to inhibition of the progress of plastic deformation by whiskers present in the matrix. However, with an increase in porosity %, the actual hardness values are overshadowed and as a result, the hardness in composite with 15% ABO_w is reduced instead of increasing. As agglomeration of whiskers proceeds in specimens with 15 wt.% ABO_w, the non-uniform sintering driving force leads to localized shrinkage strains introducing more defects (dislocations and point defects, etc.) [114-115] at the interfaces of ABO_w and

matrix during grain growth so that the interface strength decreases during sintering. This behavior of composite increases [116,117] with increasing volume fraction in aluminium matrix [115]. The samples' flexural strength was calculated using a three-point bending test, with a span of 30 mm and a crosshead speed of 0.5 mm/min (**Table 6.2**).

Table 6.2 Bending strength and Vickers hardness of samples

S. No.	Wt % of ABO_w in Al	Bending Strength at room temperature (MPa)	Hardness (HV)
1	0	125±2	27±2
2	5%	160±2	37±3
3	10%	172±2	40±5
4	15%	165±2	39±2

A linear increase of bending strength could be observed up to Al-10 wt% ABO_w (172 Mpa) but drops with a further increase in ABO% to 15 wt.% due to brittleness of the whiskers and higher porosity%. Hence, it can be inferred that the bending strength increases as a result of an increase in strength by dispersion strengthening.

6.4.2 Compression behaviour

The behavior of composites under compression are shown in the engineering stress-strain diagram in **Figure 6.6**. The maximum compressive strength (324 MPa) could be observed in composite having 10 wt.% ABO_w while decreasing the weight

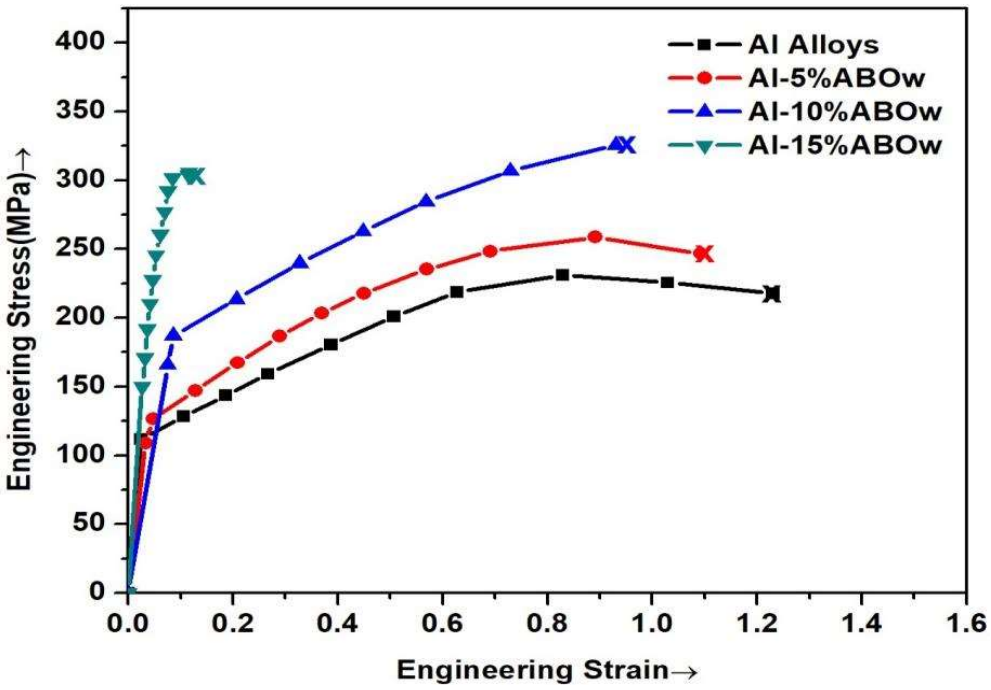

Figure 6.6: Engineering stress-strain curves of base metal and composites with different percentages of reinforcements

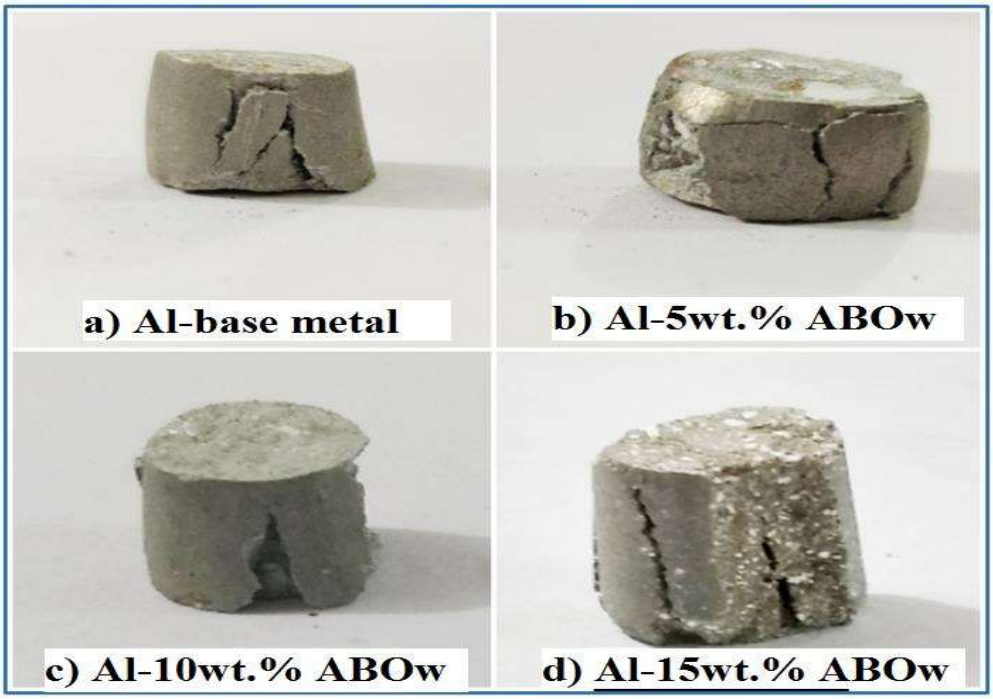

Figure 6.7: Macrographs showing longitudinal surface cracks during compressive failure of aluminium base metal and sintered Al-ABO_w composites

percentage of ABO_w the compressive strength (217 MPa) decreases. However beyond 10wt.% of ABO_w reduces compressive strength due to agglomeration of brittle ABO_w as evident with 15 wt.% addition of ABO_w. The macrographs exhibiting compressive surface failures of composites with different wt.% of ABO_w at room temperature are shown in **Figure 6.7**. Numerous longitudinal surface cracks could be observed on the surface as the percentage of ABO_w is increased.

6.5 Fracture characteristics

6.5.1 Fractography of bending failures

The typical SEM fractography of Al-ABO_w composites is exhibited in **Figure 6.8**. The base aluminium fracture without any whisker reinforcements exhibited ductile nature; the fracture propagates along the micro holes and dimples on the surface (not shown in the figure). In contrast, the fractography of Al/ABO_w composites in **Figure 6.8 (a)** depicts the predominantly brittle nature of the fracture. But, most of the whiskers remain intact in the matrix and are not dislodged from the matrix. So, it could be inferred that the matrix could transfer the load efficiently through the interfaces to the whiskers without being dislodged from the matrix. Consequently, enhanced mechanical properties were observed in this composite up to an ABO_w % of 10%. The whiskers are more or less evenly dispersed in the matrix. However, the composite with 15 wt.% of ABOw dispersion is not so uniform as revealed at very high magnification; clusters of whiskers are present at different locations. This leads to a decrease in bending strength in the composite with 15 wt.% ABO_w.

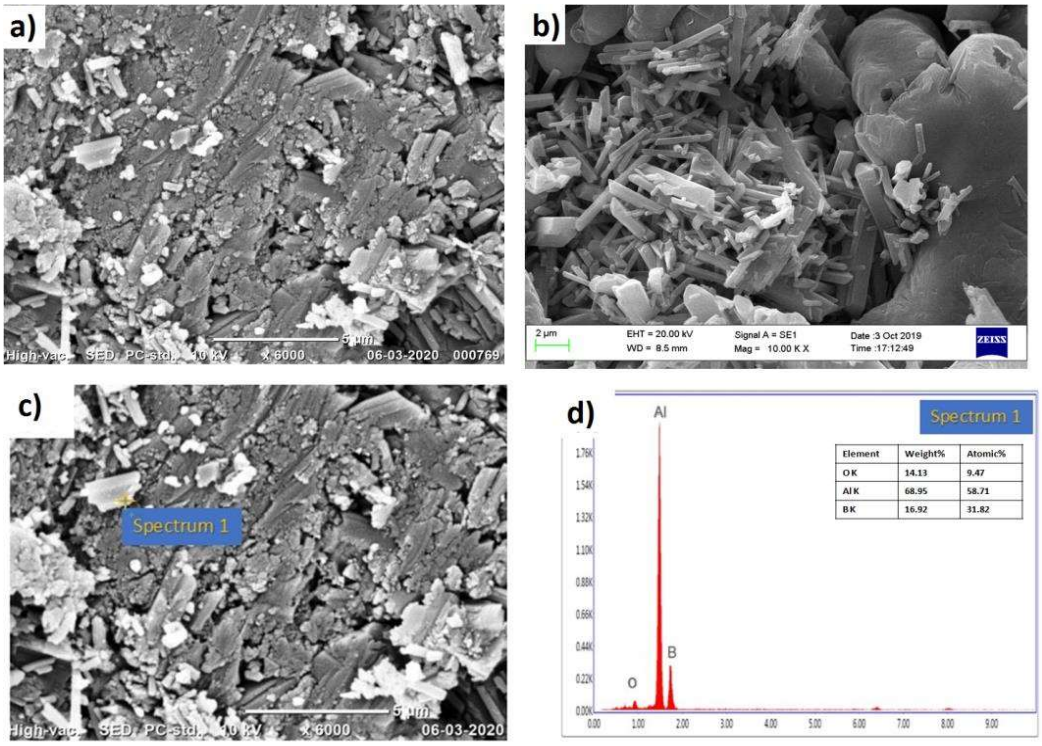

Figure 6.8: Typical fractography in bending test of (a) Al-10 wt.% ABO_w (b) Al- 15 wt.% ABO_w (c) EDS analysis point of Al-10% ABO_w (d) EDS spectrum from dislodged ABO_w

6.5.2. Fractography of compressive failures

The fractography of compressive failures of composites at low magnifications are shown in **Figure 6.9**. The compression in the aluminum base sample is ductile compared to other specimens. With an increase in the percentage of ABO_w (15%) the fracture is more brittle in nature. The characteristic of groove with many microvoids which is contributed to the motion of whisker to a certain extent, can be observed as shown in **Figure 6.9 (d)**. Certainly, the particle ABO_w is inclined to crack caused by high local stress in turn. With the higher percentage, the proportion of the region representing the flow localization increases and the matrix has to accommodate the deformation between the region of plasticity and non-plasticity. Consequently, the

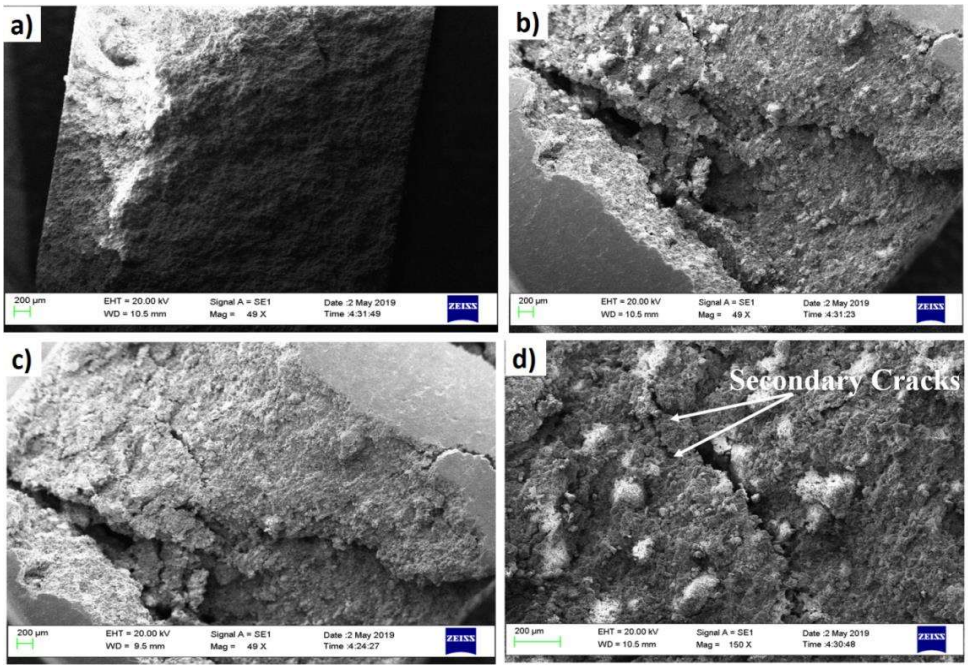

Figure 6.9: Fractography at low magnification of **(a)** aluminium base metal and composites with **(b)** 5 wt.% ABO_w **(c)** 10 wt.% ABO_w and **(d)** 15 wt.% ABO_w

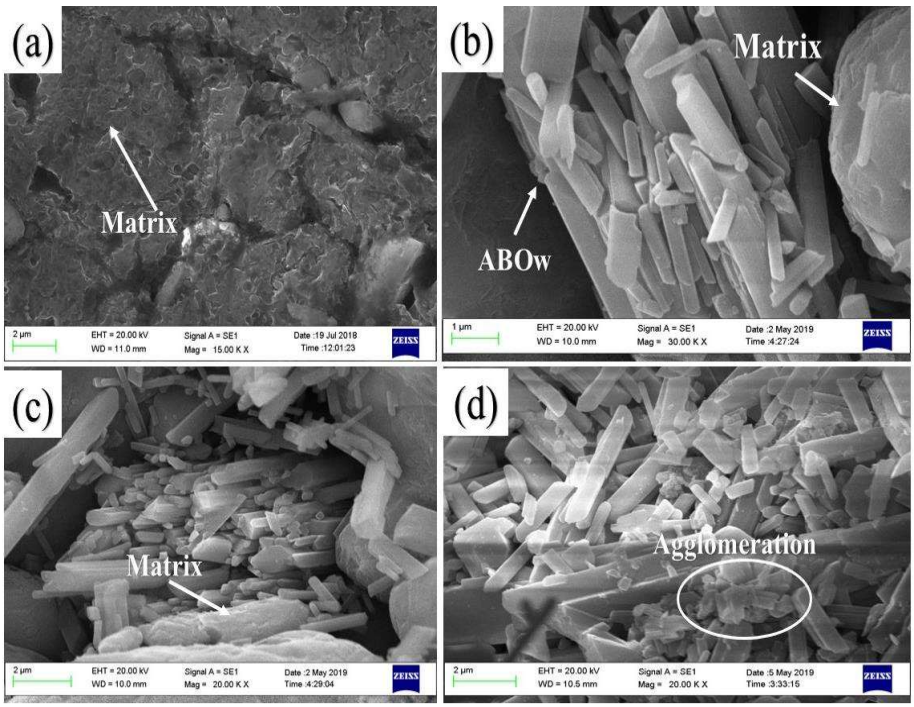

Figure 6.10: Fractography at higher magnification of **(a)** base aluminium and composites with **(b)** 5 wt.% ABO_w **(c)** 10wt.% ABO_w and **(d)** 15 wt.% ABO_w.

damage would be caused by plasticity instability. The secondary crack can manifest this as in **Figure 6.9 (d)**.The occurrence of localized plasticity signifies the improvement of the plastic deformation capacity. Nevertheless, the whole deformation process shows typical characteristics of brittle fracture. **Figure 6.10** shows the SEM micrograph after the fracture at higher magnifications, and whiskers of ABO_w are seen on the fracture surface. Some fragmentation of whiskers to smaller sizes are noticed in the samples, specifically with 15wt.% ABO_w.

6.6 Strengthening mechanisms

The combined effects of various strengthening mechanisms, namely, load transfer, thermal mismatch, and Orowan strengthening, develop the ultimate strength of the composites. The transfer of external load from matrix to reinforcements depends on the volume fraction of reinforcements and the matrix/reinforcements interface bonding [118, 119-120]. The change in compressive strength due to load transfer ($\Delta\sigma_{load}$) can be expressed as,

$$\Delta\sigma_{load} = \frac{1}{2}\sigma_m V_f [s_\theta + \frac{3\pi - 4}{3\pi}(1 + \frac{1}{s})\theta] \qquad (6.1)$$

Where, θ is the angle between the whisker orientation and the compression direction (The average angle can be considered as π/4) [154], σ_m is the yield strength of Al matrix, V_f is the volume fraction of whiskers, *s* is the average aspect ratio of ABO whiskers. The mismatch between the coefficient of thermal expansion of whisker and the aluminium matrix causes high dislocation density during cooling from the sintering temperature to room temperature. The resultant high dislocation density is expressed as,

$$\rho_t = \frac{BV_f(\alpha_m - \alpha_f)}{b(1-V_f)t}\Delta T \qquad (6.2)$$

Where, B is a geometrical constant and is equal to 10 for whiskers, b is Burger's vector. It is equal to 2.86 nm, αm and αf are the co-efficient of thermal expansions of matrix and whisker respectively and the values are 23.6 x10-6 and 2.6 x 10-6 K-1, t is the minimum size of the whiskers (0.5 μm). ΔT is the difference between sintering temperature and room temperature.

Hence, the combined effects of dislocation densities are,

$$\Delta\sigma_D = \lambda G_m b\sqrt{\rho_t} \qquad (6.3)$$

Where, λ is a constant and is equal to 1.25 and G_m is shear modulus equal to 27 GPa.

The ultimate compressive yield strength (Δσ) can be evaluated from the relationship,

$$\Delta\sigma = \sqrt{\Delta\sigma_{load}^2 + \Delta\sigma_D^2} \qquad (6.4)$$

The estimated combined yield strength of the Al-ABO_w composites with varying wt.% of ABO_w are presented in **Table 6.3**.

It is evident that, the estimated compressive yield strengths widely differ from the actual results. This is perhaps due to the agglomeration of whiskers at locations with increasing wt.% of ABO_w.

Table 6.3 Theoretical estimation of different strengthening effects

Content of ABOw /Wt.%	Strengthening due to load transfer $\Delta\sigma_{Load}$ (MPa)	Strengthening due to dislocation, $\Delta\sigma_D$ (MPa)	Total theoretical yield strength, $\Delta\sigma$ (MPa)
5%	119	140	184
10%	356	108	372
15%	415	133	434

6.7 Dry sliding wear behaviour

The wear rate versus sliding distance (time) of different Al-ABO_w composites under fixed normal load (10N) and sliding velocity (1.15 ms^{-1}) are shown in **Figure 6.11**. The wear rate of Al-ABO_w composites decreases with an increase in ABO_w content up to 10 wt.%. However, a further increase in ABO_w percent increases wear rate. Up to about 10 wt.%, the whiskers are more or less randomly distributed in the matrix, and the matrix /reinforcement interface has adequate strength to combat the wear. But the excess volume percent t of ABO_w leads to a non-uniform dispersion and forms clusters. These clusters of whiskers are easily dislodged during wear because of their weak matrix/reinforcement interface strength. The dislodged whiskers cause a three-body abrasion with further sliding of the mating surfaces. At the initial period of sliding, both 10 wt.% ABO_w, as well as 15 wt.% ABO_w, reinforced composites are showing almost the same wear rate, but as the sliding progresses, the frictional heat generated

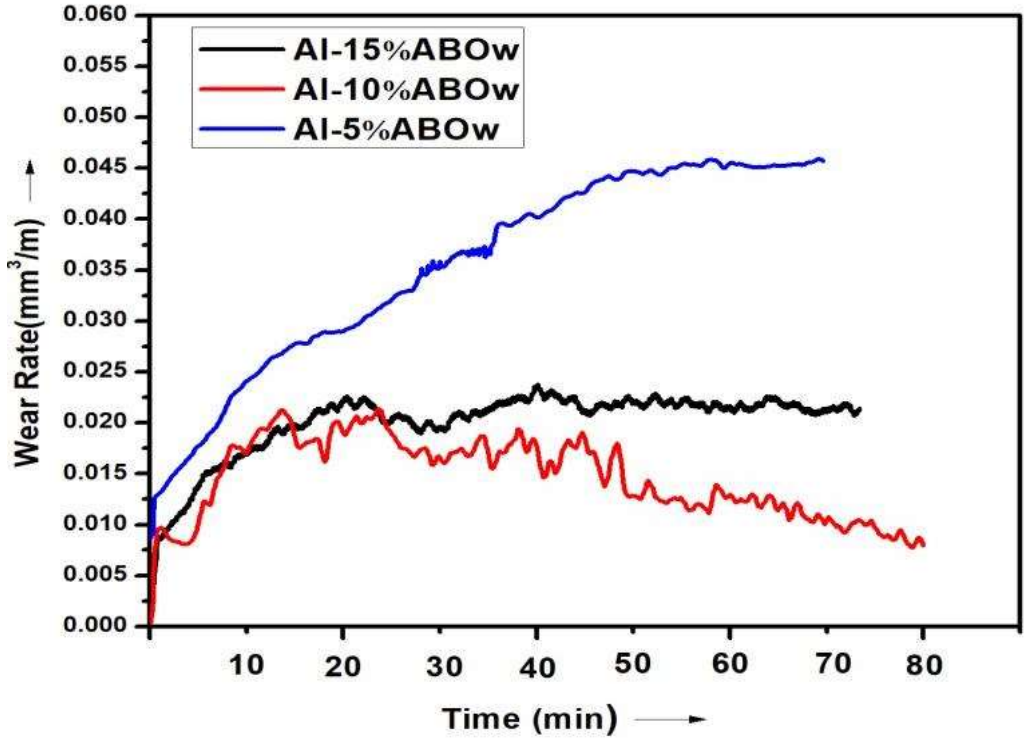

Figure 6.11: Variation in wear rate with sliding distance (time) for different wt.% ABO_w in Al matrix composites

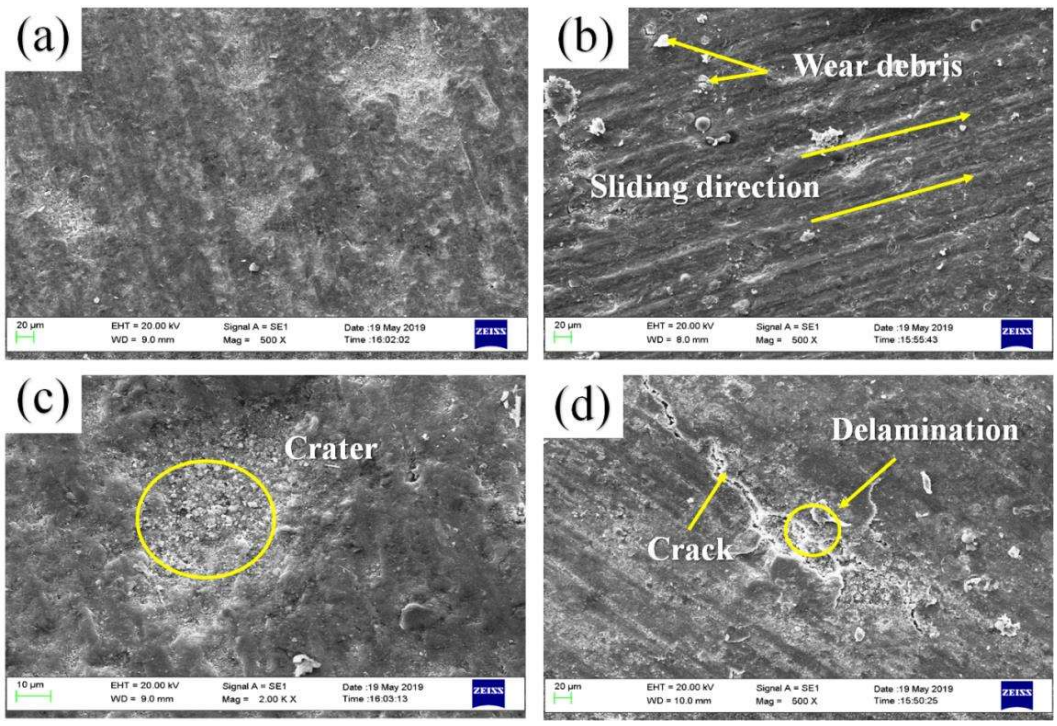

Figure 6.12: SEM images of worn surfaces of **(a)** base aluminium and composites with **(b)** 5 wt.% ABO_w **(c)** 10 wt.% ABO_w and **(d)**15wt.% ABO_w respectively

increases. The increased contact surface temperature leads to softening of the matrix, which, in turn, raises the degree of plastic deformation, aggravating the dislodging of whiskers from the matrix.The worn surface topography under SEM at maximum sliding distance traversed are shown in **Figure 6.12**. In these figures fragmentation of asperities, the formation of wear debris, and cracks and delaminations are prominent. In base metal and composite with 5%ABO_w, the sliding grooves formed are deeper because of the ploughing action of the hard steel surface asperities on a softer test sample surface. The worn surface of Al-10wt.% ABO_w composite is much smoother and almost free from wear debris. However, with 15 wt.% ABO_w, shallow surface scars with fine cracks and subsequent delamination are observed.

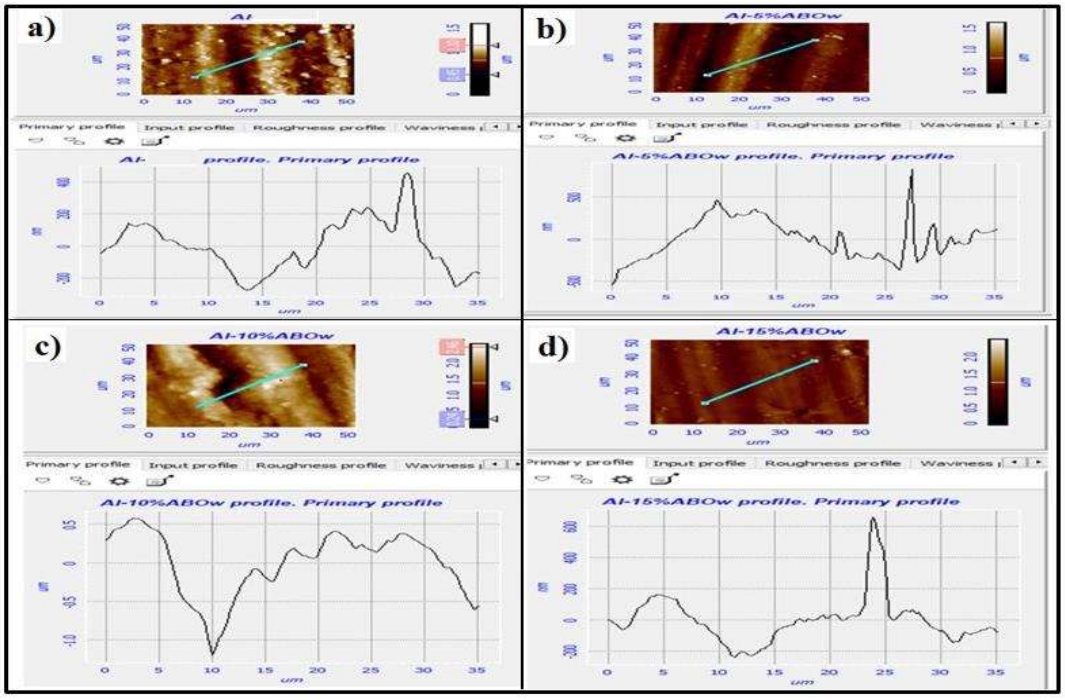

Fiure 6.13: Line analysis perpendicular to wear track and its 2D-profilometric images of **(a)** base aluminium and composites with **(b)** 5wt.% ABO_w **(c)** 10wt.% ABO_w and **(d)** 15wt.% ABO_w respectively

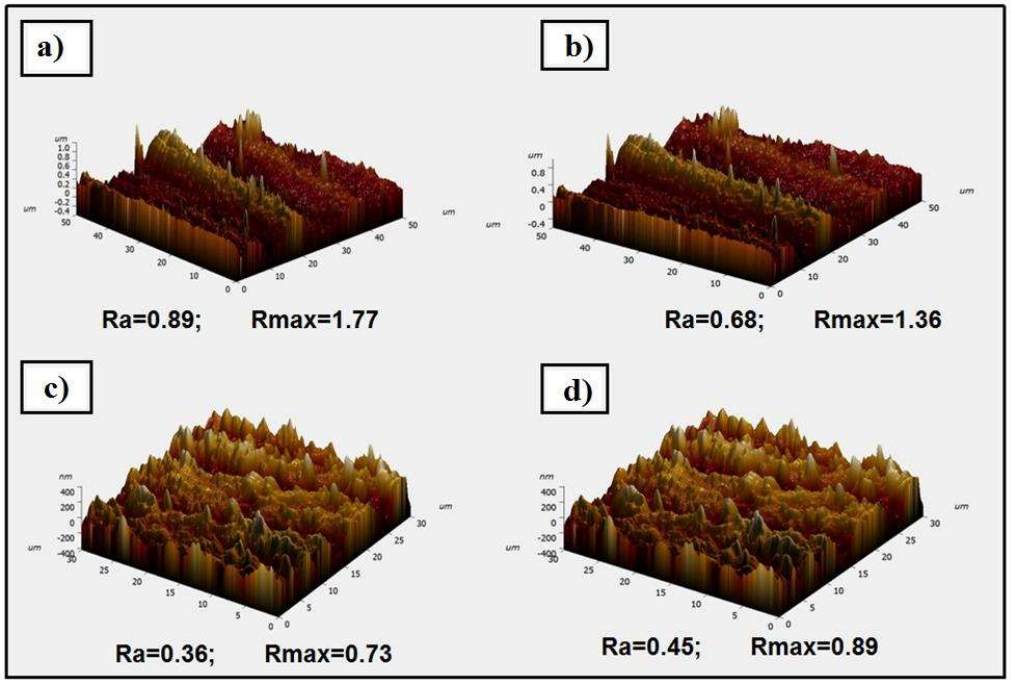

Figure 6.14: 3D-profilometric images of (a) base aluminumin and composites with **(b)** 5, **(c)** 10 and **(d)** 15wt.% ABO$_w$

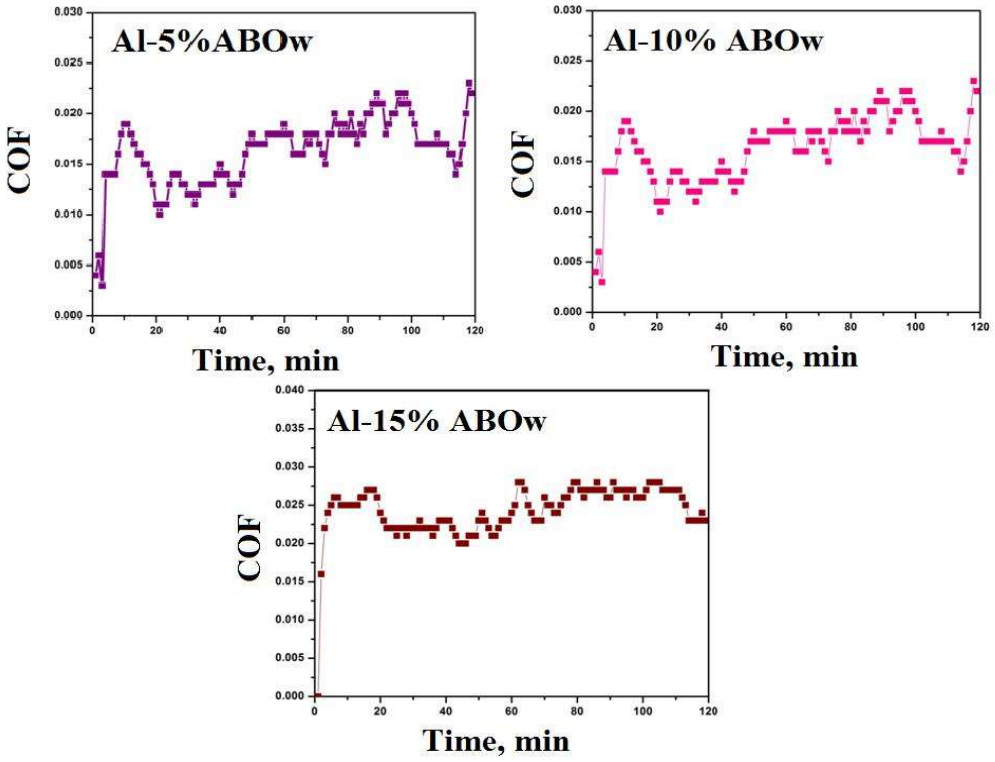

Figure 6.15: Effect of sliding distance (time) on co-efficient of friction for different percentages of ABO$_w$ in the composites

The cracks have been propagated both in longitudinal and transverse directions with respect to sliding direction. The 2D and 3D profile analysis of the worn surfaces and the surface roughness values are shown in **Figure 6.13** and **Figure 6.14,** respectively. The wear scar characteristics substantiate the SEM observations [121-124].

The surface roughness is a minimum of 10 wt.% ABO_w and increased a little bit with 15 wt.% ABO_w.The observed coefficient of friction (COF) in Al-ABO_w composites is shown in **Figure 6.15**. It is evident from the figure that the average COF values are almost similar in composites with 5% and 10% ABO_w. However, in composite with 15% ABO_w, there is a substantial increase in COF value. In the case of 15% ABO_w composite, the dislodged whiskers by the shearing action are adhered in between the two mating surfaces, increasing in COF.

6.8. Chapter summary

In the light of microstructural characterization and consequent mechanical and wear characteristics evaluation following conclusions can be drawn: The ABO whiskers are more or less uniformly dispersed in the matrix up to a whisker weight percentage of 10%, but further increase in whisker percentage leads to clustering at different places. There is no sign of matrix/whisker interface reaction after sintering of green compacts at 600°C. The composite density decreases with an increasing percentage of whisker in the matrix due to an increase in porosity with increasing whisker content.

The hardness of composites increases up to 10wt % ABO_w addition due to dispersion strengthening with reduced porosity and more interfacial bonding between matrix and reinforcement. With 15 wt.% ABO_w, effects of whisker strengthening are overshadowed by porosity %, leading to a reduction in hardness and strength. The

flexural strength is around 172 MPa and compression strength 324 MPa with 10wt.% ABO_w reinforcement was observed due to lower porosity and better reinforcement dispersion than other sintered samples. Al-10wt.% ABO_w exhibits the best dry sliding wear resistance. With 15wt.% ABO_w the whiskers are dislodged due to non-uniform dispersions forming larger quantities of debris. From microstructural characterization and the mechanical properties developed in the Al-ABO_w composites, it can be inferred that 10 wt.% whisker is optimum to yield the best ultimate properties.